Tide-induced recirculation across the aquifer-ocean interface

C. Robinson,[1] L. Li,[1,2] and H. Prommer[3]

Received 31 October 2006; revised 19 March 2007; accepted 30 March 2007; published 18 July 2007.

[1] A parametric analysis is conducted to examine the influence of tides, inland hydraulic conditions, and aquifer properties on the rate of tide-induced seawater recirculation through the nearshore aquifer. Understanding such influence is crucial for accurate prediction of subsurface chemical fluxes to coastal waters via groundwater discharge. The analysis is based on numerical simulations of density-dependent groundwater flow in a coastal aquifer subject to tidal oscillations across a sloping beach face. The results reveal that the amplitude of tidal oscillations and the inland hydraulic gradient are the primary parameters controlling the tide-induced recirculation rates. Significant tidal exchange is expected when the ratio of tidal to inland forcing is large. The horizontal tidal shoreline excursion and aquifer depth both display asymptotic behavior, influencing recirculation rates for only small values where the exchange process is limited by the potential for infiltration and shallowness of the aquifer, respectively. The analysis also indicates that tidal effects increase density-driven recirculation rates due to enhanced convective flow within the saltwater wedge.

Citation: Robinson, C., L. Li, and H. Prommer (2007), Tide-induced recirculation across the aquifer-ocean interface, *Water Resour. Res.*, *43*, W07428, doi:10.1029/2006WR005679.

1. Introduction

[2] Coastal water pollution is becoming an increasingly serious global problem due to increased anthropogenic stresses on the marine environment. Most previous studies have focused on river discharge as the main (often sole) transport pathway for land-derived chemicals into coastal waters. It is now widely recognized that chemicals entering coastal waters via submarine groundwater discharge (SGD) may also have considerable consequences on the marine ecosystem [*Johannes*, 1980; *Simmons*, 1992; *Church*, 1996; *Moore*, 1996]. However, SGD is still often neglected as it is poorly described and quantified in many coastal systems [*Burnett et al.*, 2006].

[3] SGD is broadly defined as all direct discharge of subsurface fluids across the aquifer-ocean interface [*Li et al.*, 1999; *Taniguchi et al.*, 2002; *Burnett et al.*, 2003]. As such, it comprises both terrestrially derived fresh groundwater flow (Q_f) and seawater recirculating across the aquifer-ocean interface (SGR). Direct measurements [*Robinson et al.*, 1998; *Kim et al.*, 2003; *Smith and Zawadski*, 2003; *Taniguchi and Iwakawa*, 2004] and geochemical tracer experiments [*Moore*, 1996; *Moore and Church*, 1996; *Hussain et al.*, 1999; *Crotwell and Moore*, 2003] indicate that SGR often constitutes a large portion of the total SGD. Since important reactions occur as seawater recirculates through a coastal aquifer, chemicals delivered by SGR can be as significant as chemicals transported into coastal waters by terrestrially derived SGD [*Simmons*, 1992].

[4] SGR is driven by a range of processes [*Burnett et al.*, 2003; *Gallardo and Marui*, 2006], but in the nearshore region the main mechanisms driving seawater recirculation are tides (Q_t), waves (Q_w) and density-dependent flow (Q_d, Figure 1). Measurement techniques used to quantify SGD (e.g., seepage meters, piezometers, geochemical tracers) typically provide limited insight into the dynamics of the water exchange process. Although some field studies have attempted to distinguish between "fresh" and "recycled" SGD [*Gallagher et al.*, 1996; *Kim et al.*, 2003; *Taniguchi and Iwakawa*, 2004; *Michael et al.*, 2005; *Boehm et al.*, 2006; *Burnett et al.*, 2006; *Taniguchi et al.*, 2006], the mechanisms driving recirculation and their relative contribution to total SGD rates are still not well understood. Nevertheless, this understanding is crucial for predicting magnitudes of groundwater discharge and associated chemical fluxes to coastal waters, particularly as the various SGD components have such distinct chemical compositions [*Simmons*, 1992; *Oberdorfer*, 2003]. There is a need to identify conditions for which tide, wave- and density-driven seawater recirculation are likely to be significant.

[5] The magnitude of water exchange driven by density has previously been investigated using regional-scale numerical models [*Smith and Turner*, 2001; *Destouni and Prieto*, 2003; *Smith and Zawadski*, 2003; *Smith*, 2004]. The density gradients across the transition zone of the saltwater wedge drive convective circulation through the wedge which contributes to water exchange across the interface (Q_d, Figure 1) [*Smith*, 2004]. *Destouni and Prieto* [2003] suggested that the magnitude of density-driven exchange (Q_d) is easily quantifiable as a linear function of the net fresh groundwater discharge (Q_f). However, *Smith* [2004] later presented a nondimensional parametric study which indicated that prediction of Q_d is more difficult than

[1]Environmental Engineering Division, School of Engineering, University of Queensland, St. Lucia, Queensland, Australia.
[2]Centre for Eco-Environmental Modeling, Water Resources and Hydraulic Engineering, State Key Laboratory of Hydrology, Hohai University, Nanjing, China.
[3]Land and Water, Commonwealth Scientific and Industrial Research Organisation, Wembley, Western Australia, Australia.

0043-1397/07/2006WR005679$09.00

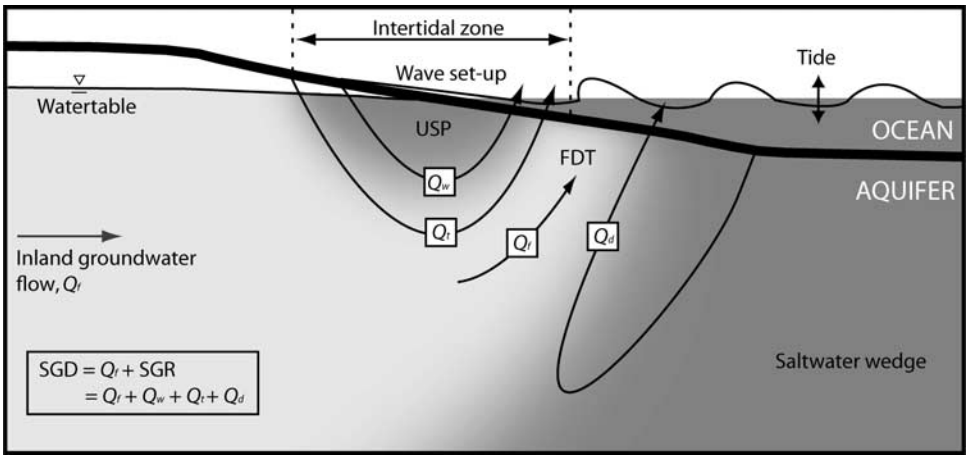

Figure 1. Conceptual model of a coastal groundwater system subject to oceanic oscillations. In the nearshore region, SGD consists of inland fresh groundwater flow (Q_f) and seawater recirculating across the aquifer-ocean interface (SGR). SGR is driven primarily by wave setup and runup (Q_w), tides (Q_t), and density-driven convection (Q_d). Shading (gray scale) depicts typical salt distribution with an upper saline plume (USP) present in addition to the classical saltwater wedge. The two saline plumes confine a freshwater discharge "tube" (FDT) whereby fresh groundwater discharges around the low-tide mark. This figure is based on Figure 1 of *Robinson et al.* [2007a] (copyright Elsevier 2007).

expected. This is due to the strong dependence of density-driven convection on the aquifer dispersivities which are typically uncertain and scale-dependent. Here, we focus on tide-induced recirculation which has received little attention but has been found to be a significant water exchange mechanism in tidally influenced environments [*Robinson et al.*, 2006].

[6] Tidal forcing across a sloping beach face results in the movement of large quantities of water (Q_t), relative to fresh groundwater discharge (Q_f), across the aquifer-ocean interface. Water infiltration occurs when the instantaneous seawater level exceeds that of the beach water table causing input on the rising tide and discharge mainly on the ebbing tide. Direct measurements of semidiurnal fluctuations in SGD are widely reported [*Reay et al.*, 1992; *Staver and Brinsfield*, 1996; *Robinson et al.*, 1998; *Kim and Hwang*, 2002; *Taniguchi*, 2002; *Taniguchi et al.*, 2003, 2005]. The nonlinearity associated with tidal forcing on a sloping beach boundary results in a tide-averaged asymmetric exchange pattern whereby infiltration dominates in the upper intertidal zone and exfiltration near the low-tide mark [*Boufadel*, 2000; *Mango et al.*, 2004; *Robinson et al.*, 2007a]. This asymmetric exchange sets up a seawater circulation cell through the intertidal zone (Figure 1).

[7] Compared with density-driven recirculation which operates over large areas and is associated with long residence times (order of $10^3 - 10^4$ d), tide-induced recirculation is a localized phenomenon characterized by high specific fluxes and relatively short residence times (order of 10^1 d) [*Robinson et al.*, 2007a]. While density-driven recirculation has the potential to drive long-term chemical exchange with aquifer sediments up to depths of kilometers below the seafloor [*Wilson*, 2005], tide-induced recirculation is typically confined to shallow intertidal sediments [*Michael et al.*, 2005; *Robinson et al.*, 2007a]. Tidally driven recirculation is significant however not only because of the chemical interaction between the recirculating seawater and sediments but more importantly because recirculating seawater may mix with fresh groundwater discharging through the nearshore aquifer. The tide-induced seawater circulation cell which operates through the intertidal zone leads to the formation of an upper saline plume in addition to the classical saltwater wedge (Figure 1) [*Boufadel*, 2000; *Vandenbohede and Lebbe*, 2005; *Robinson et al.*, 2006]. This upper saline plume represents an active and dynamic zone of mixing between the recirculating seawater (oxygenated) and fresh groundwater (anoxic), and thus an important biogeochemical reaction zone in the nearshore aquifer [*Robinson et al.*, 2007a]. Because of the importance of the mixing process in determining chemical inputs to coastal waters via SGD, this mixing and reaction zone is commonly referred to as a subterranean estuary [*Moore*, 1999; *Charette and Sholkovitz*, 2002; *Ullman et al.*, 2003; *Slomp and Cappellen*, 2004; *Spiteri et al.*, 2005; *Charette and Sholkovitz*, 2006]. The presence of the tidally driven circulation cell also results in fresh groundwater (Q_f) discharging through a freshwater "tube" near the low-tide mark, rather than at the shoreline as is the case for nontidal conditions (Figure 1) [*Robinson et al.*, 2006].

[8] Numerous models have been developed to investigate the influence of tidal forcing on the coastal groundwater system [*Oberdorfer et al.*, 1990; *Yim and Mohsen*, 1992; *Ataie-Ashtiani et al.*, 1999; *Boufadel*, 2000; *Zhang et al.*, 2001; *Chen and Hsu*, 2004; *Vandenbohede and Lebbe*, 2005]. *Li et al.* [1999] initially drew increased awareness to the significant magnitude of tide-induced seawater recirculation. On the basis of a simple theoretical model, they demonstrated that for certain conditions this recirculation may account for up to 37% of the total SGD. *Robinson and Gallagher* [1999] and *Uchiyama et al.* [2000] were first to numerically simulate and quantify magnitudes of SGD in the presence of tidal forcing. However, neither of these studies separated the "fresh" from the "recirculated" SGD components. Recent numerical investigations by *Werner*

and Lockington [2006] and *Mao et al.* [2006] provide valuable insight into the effect of tidal fluctuations on nearshore groundwater hydrodynamics and salt transport over a range of tidal, hydrological and aquifer conditions. However, quantification of the rates of exchange across the aquifer-ocean interface was not conducted in these works.

[9] Currently, the most detailed numerical investigation into the influence of tides on SGD is that of *Prieto and Destouni* [2005]. They concluded that when fresh groundwater discharge is small, tidal oscillations significantly increase the magnitude of seawater recirculation across the aquifer-ocean interface. Such a tidal effect is reduced with increasing fresh groundwater discharge. Simulations were performed for three scenarios with different aquifer thickness, hydraulic conductivity and porosity. Calculated SGD rates were found to be independent of site specifics. This result is in contrast with the findings of *Mao et al.* [2006] and *Werner and Lockington* [2006] that tide-induced flow patterns in the nearshore aquifer vary significantly for different forcing and aquifer conditions. The discrepancy may be due to the regional scale used in *Prieto and Destouni*'s model [2005].

[10] Here we present a detailed parametric study investigating the rate of water exchange across the aquifer-ocean interface driven by tidal forcing. Simulation results were analyzed using relevant nondimensional groups of physical quantities to identify conditions for which tide-induced seawater recirculation is likely to constitute a large portion of the total SGD. The density-dependent groundwater flow code SEAWAT-2000 [*Langevin et al.*, 2003] was used to conduct the numerical simulations. The magnitude of density-driven seawater recirculation in the presence of tidal forcing was also evaluated. Focusing on tidal effects, this paper does not examine seawater recirculation driven by waves [*Li et al.*, 1999], seasonal variations in the inland water table [*Michael et al.*, 2005], geothermal convection [*Kohout*, 1967] and subtidal pumping [*Riedl et al.*, 1972; *Shum and Sundby*, 1996]; these processes may also represent important mechanisms for water exchange across the aquifer-ocean interface.

2. Numerical Model

[11] The numerical model used for this study is similar to that presented by *Robinson et al.* [2007a]. Flow in an unconfined coastal aquifer subject to tidal oscillations across a sloping beach boundary is simulated using the variable-density groundwater flow code, SEAWAT-2000.

[12] SEAWAT-2000 is based on two coupled partial differential equations which describe the flow of a variable-density fluid and salt transport. The governing equation for saturated density-dependent groundwater flow is

$$\nabla \cdot \left[\rho K_f \left(\nabla \cdot h_f + \frac{\rho - \rho_f}{\rho_f} \cdot \nabla z \right) \right] = \rho S_f \frac{\partial h_f}{\partial t} + n_e \frac{\partial \rho}{\partial t} - \rho_s q_s, \tag{1}$$

where z [L] is the vertical coordinate directing upward; K_f [LT^{-1}] is the equivalent freshwater hydraulic conductivity; h_f [L] is the equivalent freshwater head; ρ [ML^{-3}] is the fluid density; ρ_f [ML^{-3}] is the freshwater density; S_f [L^{-1}] is the equivalent freshwater storage coefficient; t [T] is the time; n_e is the effective porosity; and ρ_s [ML^{-3}] and q_s [T^{-1}] are the density and flow rate per unit volume of aquifer of the source/sink, respectively [*Langevin et al.*, 2003]. The governing equation for salt transport is

$$\frac{\partial (n_e C)}{\partial t} = \nabla \cdot (n_e D \nabla C) - \nabla \cdot (n_e \vec{v} C) - q_s C_S, \tag{2}$$

where C [ML^{-3}] is the concentration of dissolved salt; D [L^2T^{-1}] is the hydrodynamic dispersion coefficient tensor; $\vec{v}$ [LT^{-1}] the pore water velocity; and C_s [ML^{-3}] is the concentration of dissolved salt from the source/sink [*Zheng and Wang*, 1999]. The relationship between the fluid density and salt concentration is represented by the linear equation of state:

$$\rho = \rho_f + \frac{\partial \rho}{\partial C} C, \tag{3}$$

where $\frac{\partial \rho}{\partial C}$ is set to 0.7143 with ρ and C both expressed in kg m^{-3} [*Langevin et al.*, 2003]. This value is applicable for salt concentrations ranging from zero to that of seawater (around 35 kg m^{-3}).

[13] A schematic of the model domain is shown in Figure 2. Alongshore groundwater flow and salt transport were assumed to be negligible and as such the model was two dimensional in the vertical and shore normal directions. The model had a total length, $L = L_S + L_L$ and an aquifer thickness, H. The x-z coordinate origin was located at the shoreline (i.e., intersection of the mean sea level with the beach face).

[14] Tidal forcing across a sloping beach face results in a highly dynamic and complex boundary along the aquifer's seaward interface. For certain conditions, the water table within a coastal aquifer may become decoupled from the tidal level during ebbing tide, leading to the formation of a seepage face where water outcrops on the beach face [*Turner*, 1993]. When this decoupling occurs the aquifer's seaward boundary consists of both a head-prescribed face and a seepage face. While the hydraulic head on the head-prescribed face is given by the tidal elevation, the seepage face is determined by the local elevation. The position and extent of the seepage face is not known a priori, making specification of this boundary condition difficult. To simulate tidal forcing on the aquifer's seaward boundary, we used a two zone model with a surface water and an aquifer zone. A sloping boundary was used to separate the two zones in the intertidal and nearshore subtidal regions. Further offshore a horizontal boundary, typical in lower-energy environments, was used to represent the aquifer-ocean interface. Coastal surface water was simulated using high hydraulic conductivity (10^6 m d^{-1}), n_e = 1 and constant salt concentration = 35 kg m^{-3}. Tidal forcing was implemented by applying temporally varying heads to specific cells in the surface water zone (Figure 2). A semidiurnal tide was simulated:

$$h_T = A \cos \omega t + H, \tag{4}$$

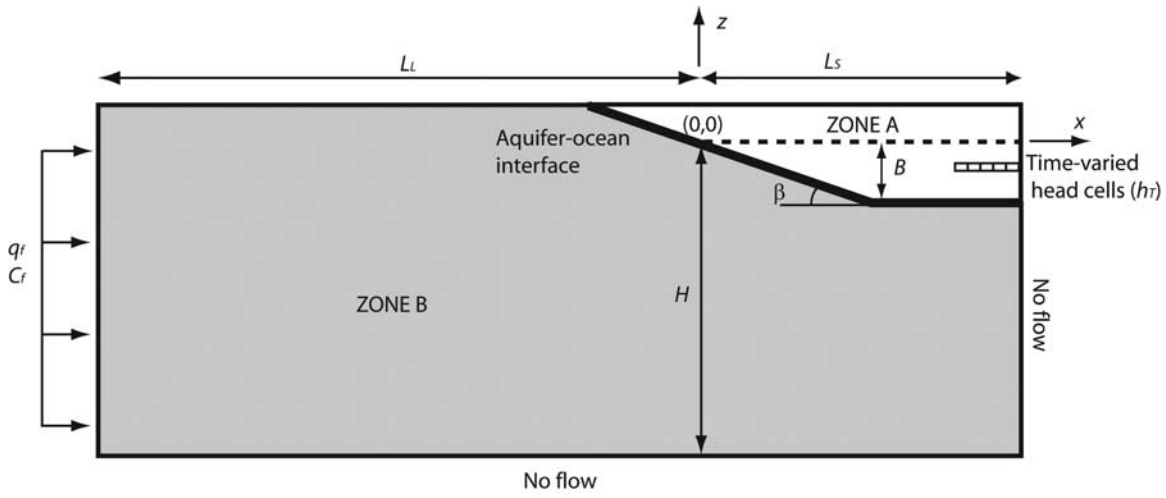

Figure 2. Model geometry and boundary conditions. Model domain is divided into two zones: a surface water zone (zone A, not shaded) and an aquifer zone (zone B, shaded). This figure is based on Figure 2 of *Robinson et al.* [2007a] (copyright Elsevier 2007).

where h_T (m) is the time-varying head, A (m) is the tidal amplitude and ω is the tidal angular frequency (12.567 d^{-1}; period = 0.5 d). The high hydraulic conductivity assigned to surface water cells allowed for nearly instantaneous transmission of this dynamic head condition to the submerged aquifer-ocean interface. The use of a high hydraulic conductivity zone for surface water has previously been adopted in groundwater models simulating seepage into lakes [*Winter*, 1976; *Anderson et al.*, 2002]. More recently this technique was employed by *Mao et al.* [2006] to model groundwater dynamics in a coastal aquifer subject to tidal forcing.

[15] While this two zone approach allowed for the simulation of tidal forcing on the aquifer's seaward boundary, it did not permit seepage face development. SEAWAT-2000 does not model variably saturated flow but uses a drying/rewetting function to model the transient dewatering of cells in response to tidal fluctuations. On the ebbing tide, a cell falls "dry" and is made inactive (i.e., no flow) when the calculated head in the cell falls below the bottom elevation of the cell. On the rising tide, the cell is "rewet" when the water levels in neighboring cells are above a user-defined threshold. As cells above the water table are no flow, discharge across the aquifer-ocean interface can only occur through the surface water cells below the tidal level (i.e., through the submerged aquifer-ocean interface). Therefore the seepage face was not simulated. As a result, we expect that for conditions where a seepage face is likely to form (e.g., flat beach, low permeability and large tidal amplitude), predicted tidal exchange rates may be underestimates due to the restricted discharge across the interface. Despite this limitation of the model, the numerical predictions provide significant insight into the magnitude of tide-induced recirculation, advancing considerably the current state of knowledge.

[16] The offshore vertical boundary was a no flow boundary. Implementation of a time-varying head (tidal) condition along this boundary did not have a noticeable effect on flows in the nearshore aquifer and subsequent SGD rates so long as the boundary was located far from the shore. Terrestrial groundwater discharge (Q_f) was simulated by specifying a uniform constant flux along the landward vertical boundary:

$$Q(-L_L) = q_f H \tag{5a}$$

$$C(-L_L) = C_f, \tag{5b}$$

where Q ($m^3\ m^{-1}\ d^{-1}$) is the volumetric discharge per unit width of the aquifer, q_f ($m\ d^{-1}$) is the uniform, specific discharge and C_f (0.1 $kg\ m^{-3}$) is the salt concentration of fresh groundwater. The bottom boundary was no flow, representing an impermeable aquifer base. The upper boundary was a phreatic surface with negligible groundwater recharge.

3. Dimensional Analysis

[17] The nearshore aquifer system may be parameterized to assist in understanding the factors controlling seawater recirculation in the presence of tidal forcing. The analysis presented below extends that by *Smith* [2004]. The system involves 16 independent quantities (L_L, L_S, H, B, β, K_x, K_z, Q_f, n_e, α_L, α_T, D_m, ρ_s, ρ_f, A, ω) which are expressed in three unit dimensions: length [L], time [T] and mass [M]. Quantities not previously defined include: offshore water depth B (m), beach slope β (dimensionless), horizontal and vertical hydraulic conductivities K_x, K_z ($m\ d^{-1}$), longitudinal and transverse dispersivities α_L, α_T (m), and coefficient of molecular diffusion D_m ($m^2\ d^{-1}$).

[18] The problem may be simplified by assuming: (1) the aquifer is isotropic and homogeneous ($K = K_x = K_z$); and (2) molecular diffusion is negligible ($D_m = 0$). This reduces the number of independent quantities to 14 (L_L, L_S, H, B, β, K, Q_f, n_e, α_L, α_T, ρ_s, ρ_f, A, ω). Buckingham's Pi Theorem [*Buckingham*, 1914] suggests that the system's behavior can be characterized using 11 (14 minus 3) nondimensional groups. Table 1 summarizes the nondimensional groups adopted in this study.

Table 1. Nondimensional Groups

Parameter	Description	Values	Quantities Varied
$L_L^* = L_L\sqrt{\frac{n_e\omega}{2KH}}$	Ratio of landward model extent to tidal propagation distance (λ)	$\geq$5	L_L
$L_S^* = L_S\sqrt{\frac{n_e\omega}{2KH}}$	Ratio of seaward model extent to tidal propagation distance (λ)	$\geq$5	L_s
$H^* = \sqrt{\frac{\omega n_e H}{2K}}$	Ratio of aquifer depth to tidal propagation distance (λ) [*Nielsen et al.*, 1997]	1.00–4.30	K, β, Q_f
$B^* = \frac{B}{H}$	Ratio of offshore water depth to aquifer depth	0.2	-
$\delta = \frac{A}{H}$	Ratio of tidal amplitude to aquifer depth	0.008–0.067	A, β
$\varepsilon = A\ cot\ \beta\sqrt{\frac{n_e\omega}{2KH}}$	Ratio of horizontal shoreline excursion to tidal propagation distance (λ) [*Li et al.*, 2000]	0–1.45	β
$Q_f^* = \frac{Q_f}{HK}$	Inland hydraulic gradient	0–0.02	Q_f
n_e	Effective porosity	0.25 (0.3, 0.35, 0.4)	n_e, K, Q_f
$D^* = \frac{H}{\alpha_t}$	Dispersion parameter [*Smith*, 2004]	60 (7.5, 15, 30, 45)	α_T, α_L
$\frac{\alpha_l}{\alpha_t}$	Dispersivity anisotropy ratio	10	-
$\rho^* = \frac{\rho_S - \rho_f}{\rho_f}$	Relative density	0.025 (0, 0.0125, 0.02)	ρ_s

3.1. Geometric Ratios (L_L^*, L_S^*, H^*, and B^*)

[19] L_L^* and L_S^* are ratios of the respective geometric lengths to the characteristic length scale, tidal propagation distance (λ). λ reflects the amplitude decay of a tide-induced groundwater wave as it propagates in the aquifer. On the basis of the small amplitude groundwater wave theory, tide-induced groundwater head fluctuations in the aquifer (h) are described by $h(-x, t) = A \exp(-kx) \cos(\omega t - kx)$ where k (m^{-1}) is the wave number, $k = \sqrt{\frac{n_e\omega}{2KH}}$ [*Nielsen*, 1990; *Li et al.*, 2004]. λ (m) is the inverse of the wave number, i.e., $\lambda = \frac{1}{k} = \sqrt{\frac{2KH}{n_e\omega}}$.

[20] Large values of L_S^* and L_L^* were chosen so that the positions of the boundaries did not influence the flows and concentrations in the nearshore aquifer. With these conditions held, the ratios were minimized to reduce the model extent and associated computational effort. The location of the landward boundary (L_L^*) was selected such that the amplitude of the local tidal groundwater wave at the boundary was damped to less than 0.1% of the tidal forcing amplitude. For all simulations this length was greater than the distance seawater intruded along the aquifer base. The seaward boundary was positioned sufficiently away from the shoreline so that its location had minimal effect on the density-driven circulations and development of the saltwater wedge. L_S^* and L_L^* were always greater than 5λ.

[21] Nondimensional aquifer depth (H^*) is the ratio of the dimensional depth (H) to the tidal propagation distance, λ. This parameter represents vertical flow effects in the aquifer. For nonshallow aquifers (i.e., larger H^*), vertical flows have been shown to introduce higher-order effects causing tidal water table fluctuations to propagate faster through the aquifer than predicted by Boussinesq type solutions [*Parlange et al.*, 1984; *Nielsen et al.*, 1997]. Here we performed a sensitivity analysis on H^* to assess the effects of this geometric parameter on the tide-induced recirculation rates.

[22] The nondimensional water depth (B^*) is the ratio of the offshore water depth (B) to the aquifer depth (H). B^* affects the location of the beach slope break; the shallower the offshore water depth, the closer the break in slope is to the shoreline. This geometric parameter was not expected to have a significant influence on recirculation rates as water exchange rapidly diminishes seaward of the low-tide mark. Thus B^* was held constant at 0.2 for all simulations.

3.2. Tidal Ratios (δ and ε)

[23] The tidal forcing on the sloping beach boundary was described by the nondimensional parameters, δ and ε. Here δ represents the tidal amplitude (A) relative to the aquifer depth (H), thus signifying the strength of the tidal forcing. ε is the ratio of the horizontal shoreline excursion ($A\cot\beta$) to the characteristic length scale (λ). These parameters have been shown to give rise to nonlinear behaviors in tidal water table fluctuations leading to the generation of higher-order harmonics and water table overheight [*Parlange et al.*, 1984; *Nielsen*, 1990; *Li et al.*, 2000]. It was hypothesized that these parameters would largely control the tide-induced recirculation rates.

3.3. Inland Hydraulic Gradient (Q_f^*)

[24] Q_f^* is the ratio of the terrestrially derived SGD (Q_f) to the aquifer transmissivity (KH). On the basis of the Ghyben-Herzberg approximation, Q_f^* (combined with ρ^*) controls the location and shape of the saltwater wedge. *Prieto and Destouni* [2005] previously investigated the effect of Q_f on SGD rates in tidally influenced systems. However, as only two tidal conditions were simulated and the tide-induced recirculation was not separated from the density-driven recirculation, their results are somewhat difficult to interpret. Here, we investigated the influence of Q_f^* over a wider range of tidal forcing conditions to better understand its influence on the magnitudes of seawater recirculation driven by tides and density.

3.4. Effective Porosity (n_e)

[25] The effective porosity n_e determines the pore volume available for the storage of solute mass and also controls the pore water velocity (v). It thus influences both the advection and dispersion terms in the salt transport equation (2). The porosity of sand typically ranges from 0.25 to 0.53 [*Zheng and Bennett*, 1995]. We used a constant n_e of 0.25. However, to test the significance of this parameter, additional simulations were performed with n_e = 0.3, 0.35 and 0.4.

3.5. Dispersion Parameters (D^* and α_L/α_T)

[26] The dispersion parameter D^* is the ratio of the aquifer depth, H, to the characteristic dispersivity parameter, α_T. Although *Smith* [2004] demonstrated that this parameter largely controls the rate of density-driven convection across the transition zone of the saltwater wedge and thus density-driven recirculation, it is not expected to have a significant influence on the tide-induced recirculation. As a result, D^* was assigned a constant value of 60. Finer grid discretization was required to control numerical dispersion in the model for larger values of D^* (i.e., grid Péclet numbers, $P_x = \Delta x/\alpha_T < 2$, $P_z = \Delta z/\alpha_T < 2$). This increased significantly the computational effort and simulation time. On the other hand, smaller values of D^* (larger α_T) led to unrealistic backward dispersion of salt into the aquifer along the discharge zone (i.e., into the freshwater discharge "tube"). This backward dispersion was an artifact of the constant salt concentration (35 kg m^{-3}) cells along the aquifer-ocean interface (i.e., in zone A) [*Robinson et al.*, 2007a]. A more realistic boundary condition would be to set the dispersive flux to zero along the outflowing portion of the boundary and constant concentration along the inflowing portion [*Smith*, 2004]. However, as the outflow zone is not known a priori, implementation of this condition is nontrivial. Notwithstanding these problems, a small number of simulations were performed to examine the effect of varying D^*.

[27] The dispersivity anisotropy ratio (α_L/α_T) was assigned a constant value = 10. Although this value falls at the lower end of the range of field-scale dispersivity estimates ($5 \leq \alpha_L/\alpha_T \leq 500$ [*Gelhar et al.*, 1992]), it was selected to minimize both numerical dispersion and backward dispersion across the interface. Previous models of density-dependent flow in coastal aquifers have also adopted this value [*Ataie-Ashtiani et al.*, 1999; *Smith*, 2004; *Prieto and Destouni*, 2005; *Wilson*, 2005]. This parameter may affect the exchange rates, in particular that of the density-driven recirculation. As this study focuses on tide-induced recirculation (an advection-dominated process), the influence of this parameter on the SGD components was not examined.

3.6. Relative Density (ρ^*)

[28] Here ρ^* was set equal to 0.025 for most simulations. This corresponds to $\rho_f = 1000$ kg m^{-3} and $\rho_s = 1025$ kg m^{-3}. Although the concentration of the surface water in a tidal estuary may be significantly lower, $C_s = 35$ kg m^{-3} (i.e., $\rho_s = 1025$ kg m^{-3}, equation (3)) is typical for ocean beaches. Here ρ^* affects the buoyancy forces which drive free convection within the saltwater wedge. As such this parameter influences the location, slope and length of the saltwater wedge transition zone. Although ρ^* was expected to affect significantly the density-driven recirculation (Q_d), it was not expected to have a large influence on tidally driven recirculation (Q_t) which is a forced convection process [*Robinson et al.*, 2007a]. This hypothesis was tested by setting ρ^* to 0, 0.0125 and 0.02.

4. Simulations and Results

[29] Simulation of tidal oscillations was computationally intensive. As a result, models were initially run to the steady state with no tide. Tidal fluctuations were then introduced and the model was run to the quasi–steady state with respect to flows across the aquifer-ocean interface. Simulations were typically run for a model time of 500 d.

[30] The model grid was nonuniform with refinement ($\Delta x = 0.3125$ m and $\Delta z = 0.0625$ m) around the aquifer-ocean interface where large parameter variations and concentration gradients existed. Tests were performed to verify that numerical solutions were independent of the grid discretization. Relative differences in the exchange rates between the predictions of the base models and more finely discretized models were within 1%. The base models had 226 columns and 151 layers.

[31] Numerical results were generated for the range of nondimensional values listed in Table 1. To identify the individual effect of parameters, one nondimensional parameter was systematically varied while all others were held constant. The physical quantities changed to vary each nondimensional parameter without modifying others are listed in Table 1. The base simulation about which the required quantities were varied had nondimensional parameters: $Q_f^* = 0.007$, $\delta = 0.033$, $\varepsilon = 0.72$ and $H^* = 2.17$. These values represent a typical tidally influenced coastal aquifer system. All simulations were conducted for a 30-m thick aquifer. This aquifer depth minimized the size of the model domain and thus computational effort, while also ensuring that D^* (H/α_T) was realistic and did not create excessive backward dispersion across the aquifer-ocean interface (see section 3.5). Simulations of deeper (60 m) and shallower (15 m, 7.5 m) aquifer systems were performed to confirm that the results were independent of the model scale.

[32] We show in Figure 3 the simulated velocities and concentrations in the nearshore aquifer at four stages of the tidal cycle (midrising, high tide, midebbing and low tide) for the base simulation. The processes revealed are indicative of those occurring when an unconfined coastal aquifer is subject to tidal forcing across a sloping beach face. Similar intratidal flow patterns have previously been shown by *Boufadel* [2000], *Ataie-Ashtiani et al.* [1999], and *Mao et al.* [2006]. For certain slope, permeability and tidal conditions, a seepage face will also form if the water table becomes decoupled from the tidal elevation on the ebbing tide; however seepage face development was not simulated in our model. Predicted exchange rates demonstrated that infiltration (inflow) occurs predominately on the late stages of the rising tide and over the high tide when the beach water table is lower than the tidal elevation. Exfiltration (outflow) dominates during the ebbing tide and continues over the early stages of the rising tide with water draining from the aquifer (Figure 4). The difference between the total exfiltration and infiltration over the tidal cycle (i.e., total net exchange) was the fresh groundwater discharge.

[33] The specific exfiltration and infiltration rates along the aquifer-ocean interface over the tidal cycle revealed three distinctive zones of exchange: tidally driven recirculation zone (TRZ), freshwater discharge zone (FDZ) and density-driven recirculation zone (DRZ, Figure 5). Tidal fluctuations across the sloping beach face drove an asymmetric exchange pattern with infiltration occurring primarily in the upper intertidal region and exfiltration closer to the low-tide mark. This asymmetric exchange led to a tide-induced seawater circulation through the intertidal region and the formation of the upper saline plume (Figure 3) [*Robinson et al.*, 2007a]. Fresh groundwater discharged

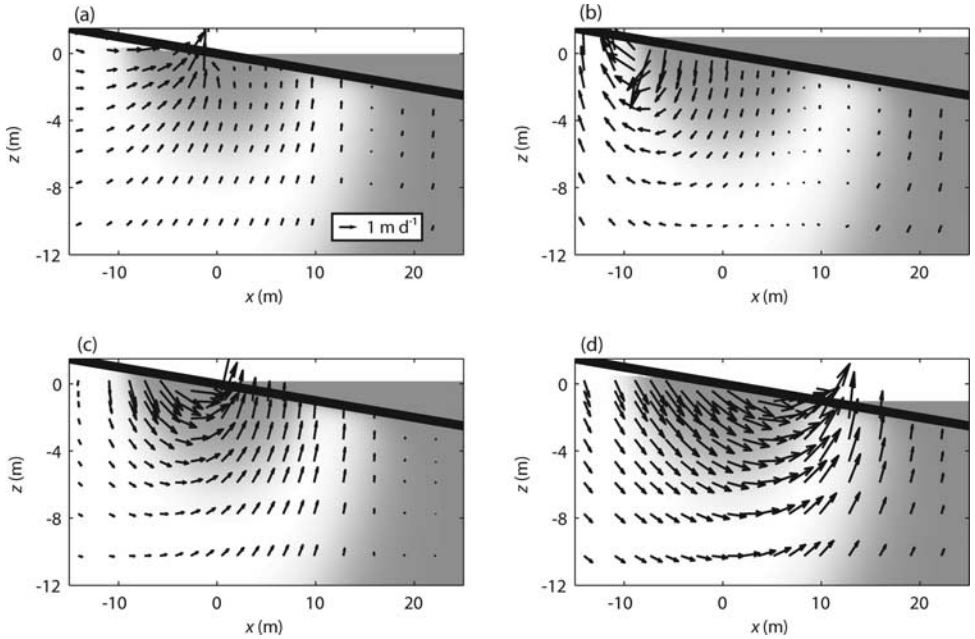

Figure 3. Flow velocities and concentrations in the nearshore aquifer at (a) midtide (rising), (b) high tide, (c) midtide (ebbing), and (d) low tide. Results are for the base simulation with $Q_f^* = 0.007$, $\delta = 0.033$, $\varepsilon = 0.72$, and $H^* = 2.17$. The diagrams focus on the area near the aquifer-ocean interface in the intertidal region. The model extent is greater than shown here with $L_S = 100$ m, $L_L = 150$ m, and $H = 30$ m. Shading (gray scale) represents the salt distribution. The scale of the velocity vectors is shown in Figure 3a.

around the low-tide mark where high exfiltration but negligible infiltration occurred. Further seaward, water exchange (infiltration and exfiltration) associated with the density-driven circulations decreased offshore.

[34] As the recirculation across the seabed is driven by two distinct mechanisms, two nondimensional parameters were defined to analyze the results: tidally driven recirculation percent (TDR),

$$\mathrm{TDR} = \frac{Q_t}{Q_f} \times 100, \tag{6a}$$

and density-driven recirculation percent (DDR),

$$\mathrm{DDR} = \frac{Q_d}{Q_f} \times 100. \tag{6b}$$

Use of two separate parameters rather than a combined recirculation percent [*Prieto and Destouni*, 2005] provides a better description of the system, allowing for understanding of the actual mechanisms controlling SGD. As the magnitude of Q_f can typically be determined on the basis of aquifer recharge, this flow was used to nondimensionalize the other SGD components. On the basis of the spatial exchange distribution shown in Figure 5, Q_t was calculated as the total infiltration across the interface landward of the freshwater discharge zone and Q_d was the total infiltration across the interface seaward of the freshwater discharge zone. A spatial exchange profile was plotted for each scenario to delineate the exchange zones.

4.1. Effect of Tidal Ratios (Variable δ and ε With Other Parameters Constant)

[35] Tidally driven recirculation percent (TDR) increases significantly as δ increases (Figure 6a). In the absence of tidal oscillations ($\delta = 0$), TDR is zero. The relationship between δ and TDR becomes relatively linear as tidal forcing intensifies. TDR reaches up to 348% for large tidal amplitude conditions (relative to the aquifer depth). When the tidal shoreline excursion across the sloping beach face (ε) is small, any increase in the width of the intertidal zone increases the tide-induced recirculation (Figure 6b). This is due to the increase in area (potential) for infiltration. However, as ε continues to increase, the small beach slope starts to limit the beach's drainage capacity and hence the

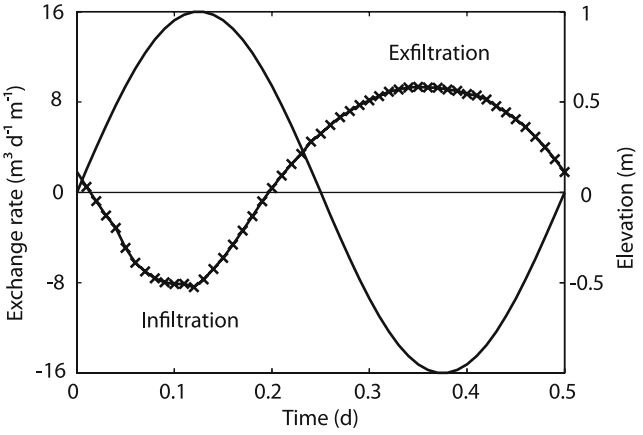

Figure 4. Temporal variations in net exchange (solid curve with crosses) across the aquifer-ocean interface through a tidal cycle (solid curve). Results are for the base simulation with $Q_f^* = 0.007$, $\delta = 0.033$, $\varepsilon = 0.72$, and $H^* = 2.17$. A positive exchange rate indicates exfiltration, whereas a negative exchange rate indicates infiltration.

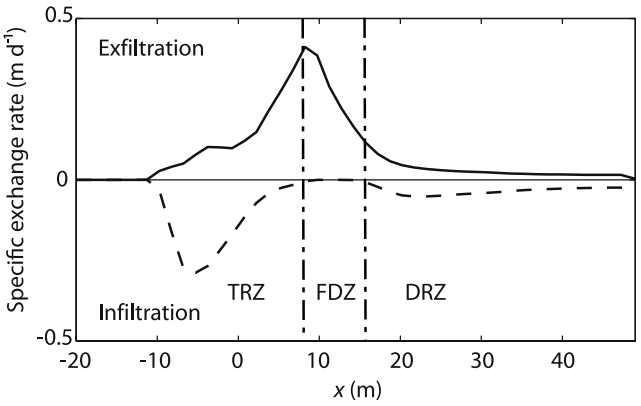

Figure 5. Specific exfiltration (solid curve) and infiltration (dashed curve) rates along the aquifer-ocean interface over a tidal cycle. Results are for the base simulation with Q_f^* = 0.007, δ = 0.033, ε = 0.72, and H^* = 2.17. The high-tide mark corresponds to $x = -10$ m, and low-tide mark corresponds to x = 10 m. The spatial behavior of infiltration along the interface reveals a tidally driven recirculation zone (TRZ) and a density-driven recirculation zone (DRZ), which are separated by a freshwater discharge zone (FDZ).

exfiltration rate, and TDR approaches an asymptotic value. For larger tidal forcing (δ) the TDR asymptote is greater.

[36] In addition to increasing the tidal exchange, δ also increases the density-driven recirculation (DDR, Figure 7). Tidal forcing enhances dispersion at the transition zone of the saltwater wedge. This leads to increased density-driven convection required to replenish salts which become entrained in the discharging fresh groundwater. In contrast, DDR decreases for increasing horizontal shoreline excursion (ε). As ε increases the tidal circulation cell operates over a wider zone with the extent of the upper saline plume increasing accordingly. The extended upper saline plume pushes the freshwater discharge zone and saltwater wedge seaward which in turn reduces the density-driven recirculation. The influence of ε on DDR is greater for larger δ as the tidal circulations (which indirectly restrict the density-driven convection) strengthen.

4.2. Effect of Inland Hydraulic Gradient (Variable Q_f^* With Other Parameters Constant)

[37] TDR decreases as the inland hydraulic gradient, Q_f^*, increases (Figure 8a). TDR however is not a suitable parameter for examining the influence of inland forcing on tidally driven recirculation rates. Varying Q_f^* ($\frac{Q_f}{KH}$) via Q_f has a direct influence on TDR ($\frac{Q_t}{Q_f} \times 100$). For example, as Q_f increases, TDR is reduced even with Q_t unchanged. To directly examine the influence of the inland condition on the tide-induced recirculation rates, Q_t may be compared for different Q_f^*. For K = 10 m d^{-1} and H = 30 m, the tide-induced recirculation rate decreases with increasing Q_f^* (Figure 8b). The tidal circulations shown in Figure 3 are pushed back in the presence of strong seaward directed fresh groundwater flow. In contrast, as Q_f^* decreases, the freshwater discharge "tube" contracts and Q_t increases as the tidal circulations expand. Q_f^* has a similar influence on Q_t for different strengths of tidal forcing (δ).

[38] The relationship between Q_f^* and density-driven recirculation (Q_d) is nonmonotonic (Figure 9). Maximum rates of Q_d are achieved for intermediate values of Q_f^*. Q_d is small for low Q_f^* because of weak density gradients across a relatively wide transition zone of the saltwater wedge [*Smith*, 2004]. As Q_f* increases the transition zone narrows causing increased convective flow and thus Q_d. For large

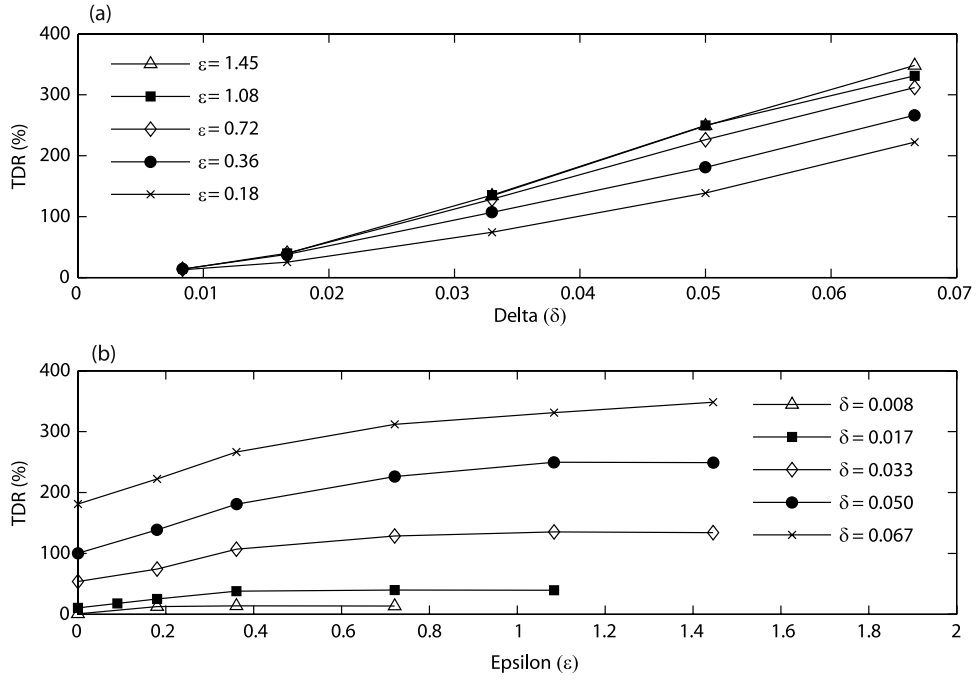

Figure 6. Effect of (a) δ and (b) ε on TDR. All other parameters are held constant: Q_f^* = 0.007 and H^* = 2.17.

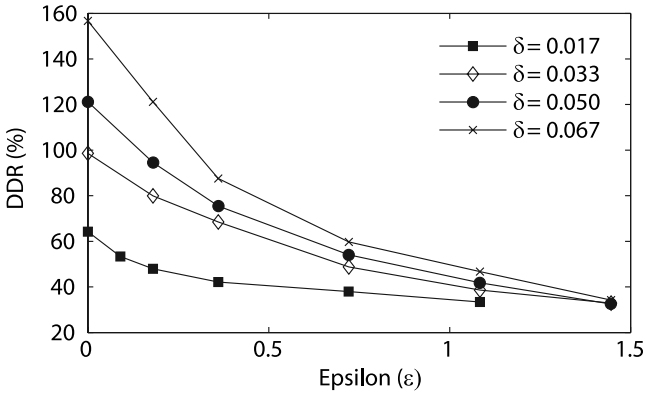

Figure 7. Effect of ε on DDR for different δ values. All other parameters are held constant: $Q_f^* = 0.007$ and $H^* = 2.17$.

Q_f^*, Q_d decreases as the extent of the seawater intrusion into the aquifer is reduced. The inland hydraulic gradient for which Q_d reaches its maximum rate increases with the tidal forcing (δ). This is due to the competing influence of tidal forcing which widens the transition zone while also reducing the extent of seawater intrusion.

4.3. Effect of Nondimensional Aquifer Depth (Variable H^* With Other Parameters Constant)

[39] Figure 10a reveals the asymptotic behavior of TDR as a function of H^*. For small H^*, the shallow aquifer depth constrains the tidally driven circulations; and increases in H^* raises TDR. However, as H^* continues to increase the finite depth effects become negligible whereby further increases no longer influence the tide-induced exchange process. The results indicate that the magnitude of density-driven recirculation is more strongly influenced by H^* than the tide-induced recirculation (Figure 10). As the aquifer depth increases, the extent of the saltwater wedge and thus area available for dispersion across the transition zone increase accordingly. This leads to enhanced convective circulation and thus increased density-driven exchange as shown in Figure 10b.

4.4. Effect of Porosity (Variable n_e With Other Parameters Constant)

[40] The results suggest that n_e has a negligible influence on TDR and DDR for the range of values (0.25 – 0.4) examined (Figure 11). Although tide- (Q_t) and density-driven (Q_d) recirculation increase as n_e increases, the fresh groundwater discharge (Q_f) also increases in direct proportion to these flows (with all other nondimensional parameters held constant). As a result, the nondimensional recirculation rates (TDR, DDR) are independent of n_e.

4.5. Effect of Dispersion Coefficient (Variable D^* With Other Parameters Constant)

[41] The dispersion coefficient D^* does not significantly affect the tidal recirculation rates (Figure 12a). D^* was varied from 7.5 – 60 and over this range TDR changed by 3.5% from 135% to 131.5%. This relative independence of TDR on D^* is not unexpected as tide-induced recirculation is an advection-dominated process.

[42] In contrast, D^* has a significant influence on the magnitude of density-driven recirculation (Figure 12b). DDR increased from 39% to 55% as D^* varied from 7.5 – 45. For D^* greater than 45, DDR reduced slightly from 55% to 53%, indicating that for the parameters simulated, the maximum DDR occurs around $D^* = 45$. This result supports the finding of *Smith* [2004] that a maximum rate of DDR is achieved for intermediate values of D^*; in his case, the optimal $D^* = 40$. He suggested that for small D^*, the density gradients across the saltwater wedge transition zone weaken as D^* decreases. This leads to a decrease in the convective overturn and hence reduced density-driven exchange. As D^* increases above the optimal value, the density-driven recirculation again decreases as the convective overturn is limited by the rate of salt dispersion across the transition zone. In this study, the range of D^* values which could be simulated was constrained by numerical considerations described in section 3.5.

5. Discussion

5.1. Conditions for Large TDR and SGR

[43] The parametric analysis revealed that δ, which represents the intensity of the tidal forcing, is the primary parameter controlling tide-induced recirculation rates (Figure 6a). To identify conditions for which seawater recirculation is likely to be significant, TDR and SGR* (nondimensional

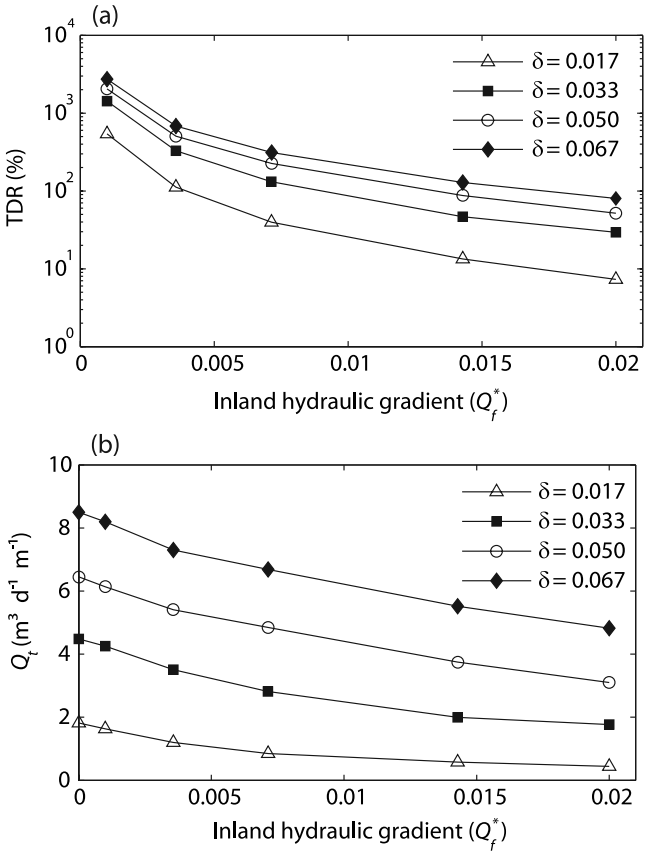

Figure 8. Effect of Q_f^* on (a) TDR and (b) tidally driven recirculation rate (Q_t) for different δ values. All other parameters are constant: $\varepsilon = 0.72$ and $H^* = 2.17$.

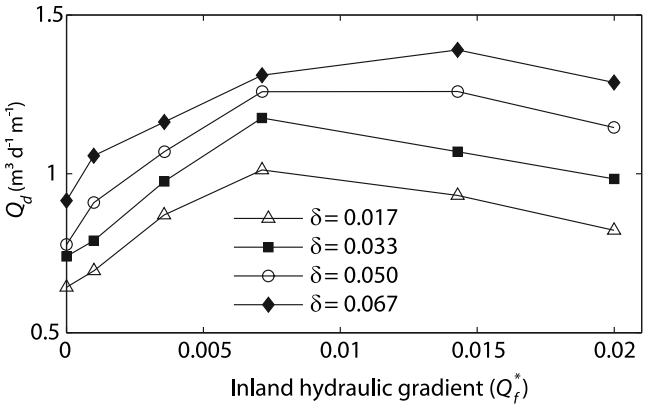

Figure 9. Effect of Q_f^* on density-driven recirculation rate (Q_d) for different δ values. All other parameters are constant: ε = 0.72 and H^* = 2.17.

SGR, $\frac{Q_t+Q_d}{Q_f} \times 100$) contours in different variable spaces are shown in Figure 13. The shaded regions represent conditions for which tidally driven recirculation (Q_t, Figures 13a–13c) and total seawater recirculation (SGR, Figures 13d–13f) are likely to contribute significantly to SGD rates (i.e., Q_t and SGR are greater than Q_f).

[44] The numerical results indicate that the inland hydraulic gradient (Q_f^*) also strongly influences the relative tidal recirculation (Figure 13a). TDR is likely to be significant on coasts with significant tidal ranges and small inland hydraulic gradients (seaward direction). The magnitude of total seawater recirculation (Q_t + Q_d) relative to the fresh groundwater discharge (Q_f) displays a similar relationship; that is, the relative recirculation is expected to be significant when the ratio of the tidal (δ) to inland forcing (Q_f^*) is large (Figure 13d). It is interesting to note that this ratio has also been shown to strongly influence the salinity stratification and extent of mixing between fresh groundwater and recirculating seawater in a subterranean estuary [*Robinson et al.*, 2007a]. Well-mixed subterranean estuaries are expected when the magnitude of tidal to inland forcing is significant; this corresponds with our finding of large seawater recirculation rates relative to fresh groundwater flow. Conversely, stratified subterranean estuaries occur when the ratio of tidal to inland forcing is small; that is, when the relative seawater recirculation is small.

[45] Figure 13b shows that ε behaves asymptotically only influencing the tide-induced exchange rate for small values (i.e., steep beaches) where the finite width of the intertidal zone restricts the exchange process. For mildly sloping beaches (larger ε), TDR contours are horizontal indicating that ε has no influence on the magnitude of tide-induced recirculation for these beaches. This is due to the competing effects of the potential for infiltration versus the beach's drainage capacity. From Figure 13e, it can be seen that the total seawater recirculation rate (SGR*) is relatively independent of ε. While tidally driven recirculation increases with increasing ε (for small ε, Figure 6b), the density-driven recirculation decreases (Figure 7); thus the effects on the two recirculation components result in a relatively constant total seawater recirculation. Although H^* was also shown to behave asymptotically (Figure 10a), the effect of aquifer thickness on TDR is small compared with δ and Q_f^* (Figure 13c). H^* has a more significant influence on the total seawater recirculation rate due to the density-driven exchange increasing with the aquifer depth (Figure 13f).

[46] On the basis of these results and the uncertainty associated with predicting actual recirculation rates, it is recommended that the magnitude of tidal forcing and inland hydraulic gradient be the primary parameters considered in assessing the relative contribution of tide-induced recirculation to total nearshore SGD rates. For steep beaches it may also be necessary to consider the horizontal shoreline excursion.

5.2. Comparison With Simulations of Field Conditions

[47] Results from simulations of two field conditions were compared with the generic modeling results presented in Figures 13a and 13d. Field studies were conducted on the west coast of Moreton Island, Australia in December 2004 [*Robinson et al.*, 2006] and July 2005 [*Robinson et al.*, 2007b]. Models were developed in SEAWAT-2000 to simulate these field conditions and the numerical results compared well with the salinity and groundwater flow data [*Robinson et al.*, 2007b]. Although ε and H^* for the field conditions do not match those for which Figures 13a and 13d were generated (i.e., ε = 1.5 and 1.3 for the December and July deployments, respectively, and H^* = 2.38 for the site), it was possible to compare the recirculation rates predicted by the field simulations as the rates are relatively independent of ε and H^* for these values (Figures 13b, 13c, 13e, and 13f). For both field deployments, δ = 0.0275. The inland hydraulic gradient was lower for the December 2004 deployment with Q_f^* = 0.003 compared with Q_f^* = 0.006 during the July 2005 deployment.

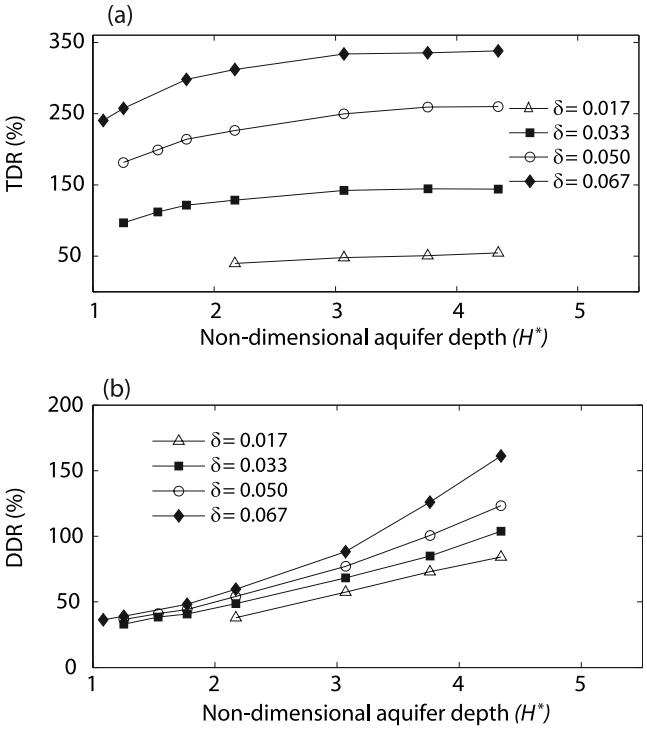

Figure 10. Effect of H^* on (a) TDR and (b) DDR for different δ values. All other parameters are constant: ε = 0.72 and Q_f^* = 0.007.

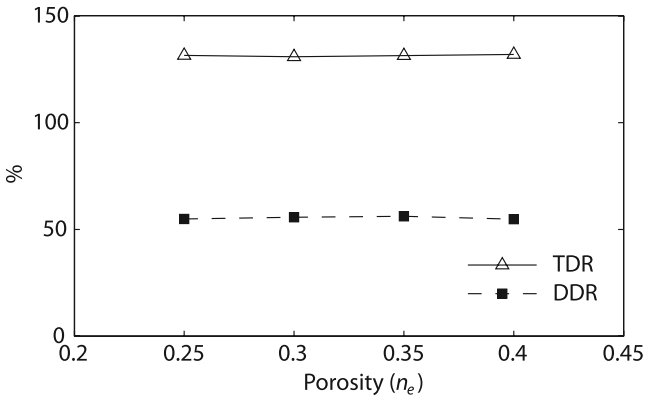

Figure 11. Effect of n_e on TDR and DDR. All other parameters are constant: $\delta = 0.033$, $\varepsilon = 0.72$, $Q_f^* = 0.007$, and $H^* = 2.17$.

The field simulations compare well with the generic numerical results. TDR and SGR* were greater when the inland forcing was reduced; TDR = 264% and SGR* = 366% for the December 2004 deployment and TDR = 132% and SGR* = 227% for the July 2005 deployment. Because of the strong influence of inland forcing, it was not possible to compare the simulation results with Figures 13b, 13c, 13e, and 13f due to the different Q_f^* values.

[48] To further validate the relationships revealed in this study, the results need to be compared with direct measurements of water exchange rates in nearshore coastal environments. Although some previous field studies have quantified and delineated between "fresh" (Q_f) and "recirculated" (SGR) discharge, it was not possible to compare these results with the relationships shown in Figure 13 as the aquifer parameters, tidal amplitude or freshwater groundwater discharge were not specified in these studies [*Kim et al.*, 2003; *Taniguchi and Iwakawa*, 2004; *Michael et al.*, 2005; *Burnett et al.*, 2006]. Knowledge of these conditions is essential for such a comparison. Also, with the exception of *Michael et al.* [2005], we are not aware of any studies which have attempted to directly measure and quantify the total tidal recirculation (Q_t) in the nearshore region. Quantifying tidal recirculation and separating this SGD component from other components requires measurement of water exchange rates and salinity within the intertidal zone.

5.3. Aquifer-Estuary Exchange

[49] Although this study focuses on aquifer-ocean exchange, groundwater discharge into coastal estuaries also represents a significant transport pathway for land-derived chemicals into the marine environment [*Smith and Turner*, 2001; *Prieto and Destouni*, 2005]. The main difference between aquifer-estuary and aquifer-ocean exchange is the salt concentration (density, equation (3)) of the receiving surface water. The driving mechanisms are the same for both cases. The salt concentrations of estuarine waters are typically less than that of the ocean (salt concentration $\approx$ 35 kg m^{-3}) because of mixing with discharging fresh riverine water.

[50] A sensitivity analysis was performed to examine the influence of the surface water salt concentration (density, ρ^*) on the exchange process. Results indicated that as the density of the surface water decreased, the convective overturn across the transition zone of the saltwater wedge is reduced, leading to a decrease in density-driven recirculation (Figure 14). DDR decreased from 52% to 0% as ρ^* decreased from 0.025 to 0 (i.e., the surface water salt concentration decreased from 35 to 0 kg m^{-3}). The density of the surface water also influenced the tidal recirculation process (Figure 14). As ρ^* decreased, the elevation of the saltwater wedge interface decreased in accordance with the Ghyben-Herzberg approximation allowing the freshwater discharge "tube" to extend downward. This reduced the upward force exerted on the tidal circulation cell by the discharging fresh groundwater. As a result, the tidal circulations expanded, enhancing tide-induced recirculation across the interface. Therefore, as the surface water freshened (35 to 0 kg m^{-3}), TDR increased from 131% to 182%. Since estuarine waters are often subject to seasonal variations in salt concentration [*Linderfelt and Turner*, 2001], these results suggest that tide- and density-driven recirculation rates (Q_t and Q_d) may also be seasonal in these environments.

5.4. Limitations of Analysis

[51] To identify the key parameters controlling recirculation in the nearshore environment, several assumptions were made to simplify the coastal aquifer system. This study only examined homogeneous, isotropic aquifers with planar beach slopes. In reality, complex beach morphology, heterogeneity and anisotropy effects will likely complicate patterns and behaviors of groundwater flow and exchange.

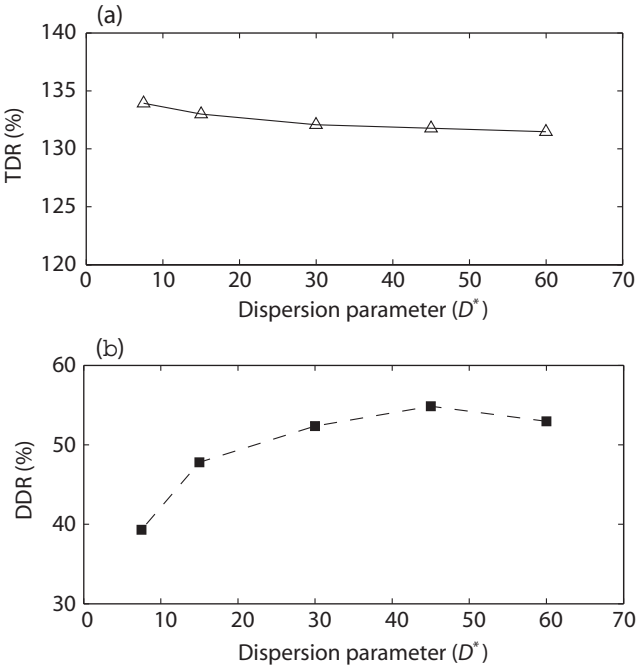

Figure 12. Effect of D^* on (a) TDR and (b) DDR. All other parameters are constant: $\delta = 0.033$, $\varepsilon = 0.72$, $Q_f^* = 0.007$, and $H^* = 2.17$.

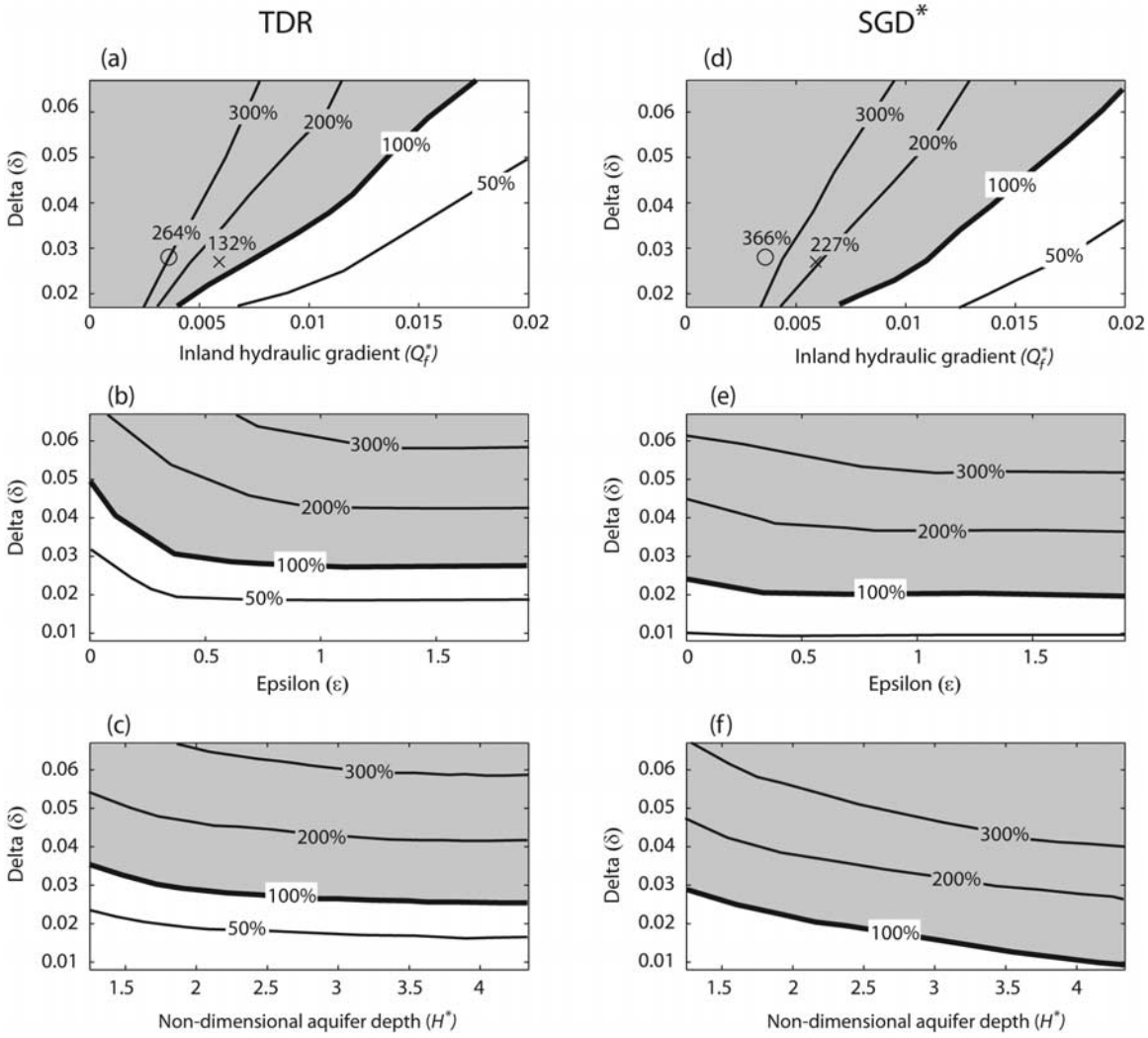

Figure 13. Contours of TDR for δ versus (a) Q_f^*, (b) ε, and (c) H^* and contours of SGR* ($\frac{Q_t+Q_d}{Q_f} \times 100$) for δ versus (d) Q_f^*, (e) ε, and (f) H^*. Where parameters are not varied, $\varepsilon = 0.72$, $Q_f^* = 0.007$, and $H^* = 2.17$. The shaded regions represent conditions for which tide-induced recirculation (Figures 13a–13c) and total seawater recirculation (13d–13f) are likely to contribute significantly to SGD rates. Conditions and relative recirculation rates for field deployments on Moreton Island in December 2004 (cross) and July 2005 (circle) are also shown in Figure 13a and 13d.

Also, temporal variations in forcing (e.g., spring-neap tidal cycle and seasonal changes in the inland hydrologic cycle) were not considered. It is expected that these cycles will drive significant fluctuations in exchange rates over their respective timescales as the relative forcing conditions vary.

[52] Focusing on tide-induced exchange, the influence of waves, which also represents an important forcing on the nearshore groundwater system, was not examined. *Longuet-Higgins* [1983] demonstrated that wave setup drives circulation with infiltration at the maximum runup point and exfiltration near the wave breaking point (Figure 1). In addition, wave runup forces infiltration into drained sediments predominantly on the rising tide [*Kang et al.*, 1994]. Waves are expected to not only significantly increase SGD in the nearshore region [*Li et al.*, 1999], but also have a marked impact on nearshore groundwater dynamics. The

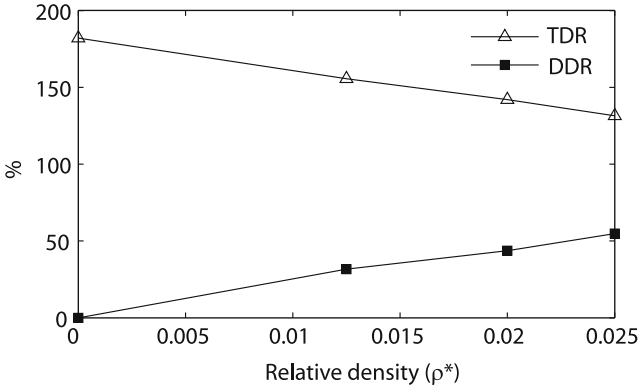

Figure 14. Effect of ρ^* on TDR and DDR. All other parameters are constant: $\delta = 0.033$, $\varepsilon = 0.72$, $Q_f^* = 0.007$, and $H^* = 2.17$.

interaction between tide- and wave-induced groundwater flows and the subsequent effect on exchange rates across the aquifer-ocean interface is an interesting and important area for future investigation.

6. Conclusions

[53] This study has demonstrated that tide-induced recirculation contributes significantly to total SGD rates in tidally influenced environments. Tidal forcing across a sloping beach results in a distinctive exchange pattern with tide-induced recirculation through the intertidal zone, fresh groundwater discharge near the low-tide mark and density-driven recirculation decreasing offshore. The parametric analysis indicated that the amplitude of tidal oscillations and the inland hydraulic gradient are the key parameters controlling tide-induced recirculation rates. Large tidal exchange is expected for conditions where the relative magnitude of the tidal to inland forcing is significant. The horizontal shoreline excursion (beach slope) and aquifer depth displayed asymptotic behavior. These parameters only influenced the tidal recirculation rate for small values where the development of the tidal circulation cell was constrained by the area available for infiltration and the shallowness of the aquifer. Simulations showed that tidal forcing also increased density-driven exchange by enhancing dispersion across the transition zone of the saltwater wedge. Maximum rates of density-driven recirculation are expected at sites with large tidal range, aquifer thickness and beach slope but intermediate inland hydraulic gradient and aquifer dispersivities.

[54] **Acknowledgments.** The authors thank C. Langevin for providing valuable assistance in using SEAWAT-2000. The research was supported by funding from Australian Research Council (DP0346461) and National Natural Science Foundation of China (50425926). Financial assistance of an Australian Postgraduate Award to the first author is also gratefully acknowledged. Comments from three anonymous reviewers have led to improvement of the paper.

References

Anderson, M. P., R. J. Hunt, J. T. Krohelski, and K. Chung (2002), Using high hydraulic conductivity nodes to simulate seepage lakes, *Groundwater*, *40*(2), 117–122.

Ataie-Ashtiani, B., R. E. Volker, and D. A. Lockington (1999), Tidal effects on sea water intrusion in unconfined aquifers, *J. Hydrol.*, *216*, 17–31.

Boehm, A. B., A. Paytan, G. G. Shellenbarger, and K. A. Davis (2006), Composition and flux of groundwater from a California beach aquifer: Implications for nutrient supply to the surf zone, *Cont. Shelf Res.*, *26*(2), 269–282, doi:10.1016/j.csr.2005.11.008.

Boufadel, M. C. (2000), A mechanistic study of nonlinear solute transport in a groundwater-surface water system under steady state and transient hydraulic conditions, *Water Resour. Res.*, *36*(9), 2549–2565.

Buckingham, E. (1914), On physically similar systems: Illustrations of the use of dimensional equations, *Phys. Rev.*, *4*, 345–376.

Burnett, W. C., H. Bokuniewicz, M. Huettel, W. S. Moore, and M. Taniguchi (2003), Groundwater and pore water inputs to the coastal zone, *Biogeochemistry*, *66*, 3–33.

Burnett, W. C., et al. (2006), Quantifying submarine groundwater discharge in the coastal zone via multiple methods, *Sci. Total Environ.*, *367*, 498–543, doi:10.1016/j.scitotenv.2006.05.009.

Charette, M. A., and E. R. Sholkovitz (2002), Oxidative precipitation of groundwater-derived ferrous iron in the subterranean estuary of a coastal bay, *Geophys. Res. Lett.*, *29*(10), 1444, doi:10.1029/2001GL014512.

Charette, M. A., and E. R. Sholkovitz (2006), Trace element cycling in a subterranean estuary: Part 2. Geochemistry of the pore water, *Geochim. Cosmochim. Acta*, *70*, 811–826, doi:10.1016/j.gca.2005.10.019.

Chen, B. F., and S. M. Hsu (2004), Numerical study of the tidal effects on seawater intrusion in confined and unconfined aquifers by time independent finite difference method, *J. Waterw. Port Coastal Ocean Eng.*, *130*(4), 191–206.

Church, T. (1996), An underground route for the water cycle, *Nature*, *380*, 579–580.

Crotwell, A. M., and W. S. Moore (2003), Nutrient and radium fluxes from submarine groundwater discharge to Port Royal Sound, South Carolina, *Aquat. Geochem.*, *9*, 191–208.

Destouni, G., and C. Prieto (2003), On the possibility for generic modelling of submarine groundwater discharge, *Biogeochemistry*, *66*, 171–186.

Gallagher, D. L., A. M. Dietrich, W. G. Reay, M. C. Hayes, and G. M. Simmons (1996), Ground water discharge of agricultural pesticides and nutrients to estuarine surface water, *Ground Water Monit. Rem.*, *16*(1), 118–129.

Gallardo, A. H., and A. Marui (2006), Submarine groundwater discharge: An outlook of recent advances and current knowledge, *Geo Mar. Lett.*, *26*(2), 102–113.

Gelhar, L. W., C. Welty, and K. R. Rehfeldt (1992), A critical review of data on field-scale dispersion in aquifers, *Water Resour. Res.*, *28*(7), 1955–1974.

Hussain, N., T. M. Church, and G. Kim (1999), Use of ^{222}Rn and ^{226}Ra to trace groundwater discharge into Chesapeake Bay, *Mar. Chem.*, *65*, 127–134.

Johannes, R. E. (1980), The ecological significance of the submarine discharge of groundwater, *Mar. Ecol. Prog. Ser.*, *3*, 365–373.

Kang, H.-Y., P. Nielsen, and D. J. Hanslow (1994), Watertable overheight due to wave runup on a sandy beach, in *Coastal Engineering 1994: Proceedings of the Twenty-Fourth International Conference*, edited by B. L. Edge, pp. 2115–2124, Am. Soc. of Civ. Eng., Reston, Va.

Kim, G., and D. Hwang (2002), Tidal pumping of groundwater into the coastal ocean revealed from submarine ^{222}Rn and CH_4 monitoring, *Geophys. Res. Lett.*, *29*(14), 1678, doi:10.1029/2002GL015093.

Kim, G., K.-K. Lee, K.-S. Park, D.-W. Hwang, and H.-S. Yang (2003), Large submarine groundwater discharge (SGD) from a volcanic island, *Geophys. Res. Lett.*, *30*(21), 2098, doi:10.1029/2003GL018378.

Kohout, F. A. (1967), Ground-water flow and the geothermal regime of the Floridian Plateau, *Trans. Gulf Coast Assoc. Geol. Soc*, *17*, 339–354.

Langevin, C., W. B. Shoemaker, and W. Guo (2003), Modflow-2000, The U. S. Geological Survey modular ground-water model—Documentation of the Seawat-2000 version with the variable density flow process (VDF) and the integrated MT3DMS transport process (IMT), *U. S. Geol. Surv. Open File Rep.*, *03-426*, 57 pp.

Li, L., D. A. Barry, F. Stagnitti, and J.-Y. Parlange (1999), Submarine groundwater discharge and associated chemical input to a coastal sea, *Water Resour. Res.*, *35*(11), 3252–3259.

Li, L., D. A. Barry, F. Stagnitti, J. Y. Parlange, and D. S. Jeng (2000), Beach water table fluctuations due to spring-neap tides: Moving boundary effects, *Adv. Water Resour.*, *23*, 817–824.

Li, L., D. A. Barry, D. S. Jeng, and H. Prommer (2004), Tidal dynamics of groundwater flow and contaminant transport in coastal aquifers, in *Coastal Aquifer Management: Monitoring, Modelling and Case Studies*, edited by A. H. D. Cheng and D. Ouazar, pp. 115–141, Lewis, Boca Raton, Fla.

Linderfelt, W. R., and J. V. Turner (2001), Interaction between shallow groundwater, saline surface water and nutrient discharge in a seasonal estuary: The Swan-Canning system, *Hydrol. Processes*, *15*, 2631–2653.

Longuet-Higgins, M. S. (1983), Wave set-up, percolation and undertow in the surf zone, *Proc. R. Soc. London, Ser. A*, *390*, 283–291.

Mango, A. J., M. W. Schmeeckle, and D. J. Furbish (2004), Tidally induced groundwater circulation in an unconfined coastal aquifer modeled with a Hele-Shaw cell, *Geology*, *32*(3), 233–236.

Mao, X., P. Enot, D. A. Barry, L. Li, A. Binley, and D.-S. Jeng (2006), Tidal influence on behaviour of a coastal aquifer adjacent to a low-relief estuary, *J. Hydrol.*, *327*, 110–127, doi:10.1016/j.jhydrol.2005.11.030.

Michael, H. A., A. E. Mulligan, and C. F. Harvey (2005), Seasonal oscillations in water exchange between aquifers and the coastal ocean, *Nature*, *436*, 1145–1148, doi:10.1038/nature03935.

Moore, W. S. (1996), Large groundwater inputs to coastal waters revealed by ^{226}Ra enrichments, *Nature*, *380*, 612–614.

Moore, W. S. (1999), The subterranean estuary: A reaction zone of ground water and sea water, *Mar. Chem.*, *65*, 111–125.

Moore, W. S., and T. Church (1996), Submarine groundwater discharge. Reply to Younger, *Nature*, *382*, 122.

Nielsen, P. (1990), Tidal dynamics of the water table in beaches, *Water Resour. Res.*, *26*(9), 2127–2134.

Nielsen, P., R. Aseervatham, J. D. Fenton, and P. Perrochet (1997), Groundwater waves in aquifers of intermediate depths, *Adv. Water Resour.*, *20*, 37–43.

Oberdorfer, J. (2003), Hydrogeologic modeling of submarine groundwater discharge: Comparison to other quantitative methods, *Biogeochemistry*, *66*, 159–169.

Oberdorfer, J. A., P. J. Hogan, and R. W. Buddemeier (1990), Atoll island hydrogeology: Flow and freshwater occurrence in a tidally dominated system, *J. Hydrol.*, *120*, 327–340.

Parlange, J. Y., F. Stagnitti, J. L. Starr, and R. D. Braddock (1984), Free surface flow in porous media and periodic solution of shallow-flow approximation, *J. Hydrol.*, *70*, 251–263.

Prieto, C., and G. Destouni (2005), Quantifying hydrological and tidal influences on groundwater discharges into coastal waters, *Water Resour. Res.*, *41*, W12427, doi:10.1029/2004WR003920.

Reay, W. G., D. L. Gallagher, and G. M. Simmons (1992), Groundwater discharge and its impacts on surface water quality in Chesapeake Bay inlet, *Water Resour. Bull.*, *28*(6), 1121–1134.

Riedl, R. J., N. Huang, and R. Machan (1972), The subtidal pump: A mechanism of interstitial water exchange by wave action, *Mar. Biol.*, *13*, 210–221.

Robinson, C., B. Gibbes, and L. Li (2006), Driving mechanisms for groundwater flow and salt transport in a subterranean estuary, *Geophys. Res. Lett.*, *33*, L03402, doi:10.1029/2005GL025247.

Robinson, C., L. Li, and D. A. Barry (2007a), Effect of tidal forcing on a subterranean estuary, *Adv. Water Resour.*, *30*, 851–865, doi:10.1016/j.advwatres.2006.07.006.

Robinson, C., B. Gibbes, H. Carey, and L. Li (2007b), Salt-freshwater dynamics in a subterranean estuary over a spring-neap tidal cycle, *J. Geophys. Res.*, doi:10.1029/2006JC003888, in press.

Robinson, M. A., and D. L. Gallagher (1999), A model of groundwater discharge from an unconfined aquifer, *Ground Water*, *37*, 80–87.

Robinson, M. A., D. Gallagher, and W. Reay (1998), Field observations of tidal and seasonal variations in groundwater discharge to tidal estuarine surface water, *Ground Water Monit. Rem.*, *18*(1), 83–92.

Shum, K. T., and B. Sundby (1996), Organic matter processing in continental shelf sediments—The subtidal pump revisited, *Mar. Chem.*, *53*, 81–87.

Simmons, G. M. (1992), Importance of submarine groundwater discharge (SGWD) and seawater cycling to material flux across the sediment/water interfaces in marine environments, *Mar. Ecol. Prog. Ser.*, *84*, 173–184.

Slomp, C. P., and P. V. Cappellen (2004), Nutrient inputs to the coastal ocean through submarine groundwater discharge: Controls and potential impact, *J. Hydrol.*, *295*, 64–86, doi:10.1016/j.jhydrol.2004.02.018.

Smith, A. J. (2004), Mixed convection and density-dependent seawater circulation in coastal aquifers, *Water Resour. Res.*, *40*, W08309, doi:10.1029/2003WR002977.

Smith, A. J., and J. V. Turner (2001), Density-dependent surface water-groundwater interaction and nutrient discharge in the Swan-Canning Estuary, *Hydrol. Processes*, *15*, 2595–2616.

Smith, L., and W. Zawadski (2003), A hydrogeologic model of submarine groundwater discharge: Florida intercomparison experiment, *Biogeochemistry*, *66*, 95–110.

Spiteri, C., P. Regnier, C. P. Slomp, and M. A. Charette (2005), pH-dependent iron oxide precipitation in a subterranean estuary, *J. Geochem. Explor.*, *88*, 399–403, doi:10.1016/j.gexplo.2005.08.084.

Staver, K. W., and R. B. Brinsfield (1996), Seepage of groundwater nitrate from a riparian agroecosystem into the Wye River estuary, *Estuaries*, *19*(2B), 359–370.

Taniguchi, M. (2002), Tidal effects on submarine groundwater discharge into the ocean, *Geophys. Res. Lett.*, *29*(12), 1561, doi:10.1029/2002GL014987.

Taniguchi, M., and H. Iwakawa (2004), Submarine groundwater discharge in Osaka Bay, *Limnology*, *5*, 25–32.

Taniguchi, M., W. C. Burnett, J. E. Cable, and J. V. Turner (2002), Investigation of submarine groundwater discharge, *Hydrol. Processes*, *16*, 2115–2129, doi:10.1002/hyp.1145.

Taniguchi, M., W. C. Burnett, C. F. Smith, R. J. Paulsen, D. O'Rourke, S. L. Krupa, and J. L. Christoff (2003), Spatial and temporal distributions of submarine groundwater discharge rates obtained from various types of seepage meters at a site in the Northeastern Gulf of Mexico, *Biogeochemistry*, *66*, 35–53.

Taniguchi, M., T. Ishitobi, and K. Saeki (2005), Evaluation of time-space distributions of submarine groundwater discharge, *Ground Water*, *43*, 336–342.

Taniguchi, M., T. Ishitobi, and J. Shimada (2006), Dynamics of submarine groundwater discharge and freshwater-seawater interface, *J. Geophys. Res.*, *111*, C01008, doi:10.1029/2005JC002924.

Turner, I. L. (1993), Water table outcropping on macro-tidal beaches: A simulation model, *Mar. Geol.*, *115*, 227–238.

Uchiyama, Y., K. Nadaoka, P. Rolke, K. Adachi, and H. Yagi (2000), Submarine groundwater discharge into the sea and associated nutrient transport in a sandy beach, *Water Resour. Res.*, *36*(6), 1467–1479.

Ullman, W. J., B. Chang, D. C. Miller, and J. A. Madsen (2003), Groundwater mixing, nutrient diagenesis, and discharges across a sandy beachface, Cape Henlopen, Delaware (USA), *Estuarine Coastal Shelf Sci.*, *57*, 539–552.

Vandenbohede, A., and L. Lebbe (2005), Occurrence of salt water above fresh water in dynamic equilibrium in a coastal groundwater flow system near De Panne, Belgium, *Hydrogeol. J.*, *14*(4), 462–472, doi:10.1007/s10040-005-0446-5.

Werner, A. D., and D. A. Lockington (2006), Tidal impacts on riparian salinities near estuaries, *J. Hydrol.*, *328*, 511–522, doi:10.1016/j.jhydrol.2005.12.011.

Wilson, A. M. (2005), Fresh and saline groundwater discharge to the ocean: A regional perspective, *Water Resour. Res.*, *41*, W02016, doi:10.1029/2004WR003399.

Winter, T. C. (1976), Numerical simulation analysis of the interaction of lakes and groundwater, *U. S. Geol. Surv. Prof.*, *1001*.

Yim, C. S., and M. F. N. Mohsen (1992), Simulation of tidal effects on contaminant transport in porous media, *Ground Water*, *30*, 78–86.

Zhang, Q., R. E. Volker, and D. A. Lockington (2001), Influence of seaward boundary condition on contaminant transport in unconfined coastal aquifers, *J. Contam. Hydrol.*, *49*, 201–215.

Zheng, C., and G. D. Bennett (1995). *Applied Contaminant Transport Modeling: Theory and Practice*, Van Nostrand Reinhold, New York.

Zheng, C., and M. C. Wang (1999), MT3DMS-A modular three-dimensional multispecies transport model for simulation of advection, dispersion and chemical reactions of contaminant in ground-water systems; documentation and user's guide, *Contract Rep.SERDP-99-1*, U. S Army Corps of Eng., Washington, D. C.

L. Li, Centre for Eco-Environmental Modeling, Water Resources and Hydraulic Engineering, State Key Laboratory of Hydrology, Hohai University, Nanjing 210098, China.

H. Prommer, Land and Water, Commonwealth Scientific and Industrial Research Organisation, Private Bag No. 5, Wembley, WA 6913, Australia.

C. Robinson, Environmental Engineering Division, School of Engineering, University of Queensland, St. Lucia, Qld 4072, Australia. (clare.robinson@epfl.ch)